by H. K. Heinrich

# Picosecond noninvasive optical detection of internal electrical signals in flip-chip-mounted silicon integrated circuits

This paper reviews the charge-sensing optical probing system, and shows how it may be used to detect internal current and voltage signals in flip-chip-mounted silicon integrated circuits. Previously, researchers have used this concept to detect both single-shot 200-MHz-bandwidth signals, without averaging, and 8-GHz-bandwidth stroboscopic signals. This system has a high sensitivity: 145-nA/√Hz current sensitivity in typical bipolar transistors, and

<sup>©</sup>Copyright 1990 by International Business Machines Corporation. Copying in printed form for private use is permitted without payment of royalty provided that (1) each reproduction is done without alteration and (2) the *Journal* reference and IBM copyright notice are included on the first page. The title and abstract, but no other portions, of this paper may be copied or distributed royalty free without further permission by computer-based and other information-service systems. Permission to *republish* any other portion of this paper must be obtained from the Editor.

1.35-mV/√Hz voltage sensitivity in typical CMOS circuits (using a semiconductor laser probe). It is noninvasive, has a potential submicron spatial resolution, and should be capable of providing linear and calibrated measurements. Therefore, this probing approach should be a powerful tool for future circuit analysis and testing.

#### 1. Introduction

As the bandwidth of silicon integrated circuits (ICs) increases beyond a few GHz, they become more difficult to test and debug. High-speed silicon emitter-coupled logic (ECL) gates have been demonstrated with switching speeds of only 23 ps [1]. High-frequency (>18 GHz) electrical probes [2, 3] have been demonstrated that can stimulate and measure these circuits. However, the probe dimensions are large compared to the internal nodes in

the circuit. Hence, mechanical-contact electrical measurement techniques only have access to test points and output nodes in the circuit.

Noncontact, nonloading, front-side probing techniques have been demonstrated [3–8] that have both high spatial and high temporal resolution. All of these techniques require access to the metal lines on the circuit. Since high-performance ICs generally have multiple layers of metal [9], these probing approaches require that test points connected to critical nodes in the circuit be provided. Hence, front-side noncontact probing approaches also have limited access to the internal nodes in the circuit.

In order to preserve the performance of high-speed ICs, these circuits are often packaged with the circuit side down, or flip-chip mounted [10–12]. In this configuration, test points to the output pads of the circuit can be provided by external contact points, which can be measured with either a high-speed electrical or a noncontact probe. Unfortunately, the long electrical leads associated with these contacts occupy a substantial amount of space in the package and degrade the circuit's switching performance. Therefore, future requirements of high-performance ICs and packages may result in a situation where ICs cannot be adequately tested by current methods.

Many of these difficulties may be overcome by probing the circuit through the back side. Back-side probing techniques provide access to any internal node in the circuit and require no circuit modifications or external contact points. Previously, back-side probing was performed by a technique referred to as optical-beam-induced currents (OBIC) [13]. In this technique, electronhole pairs are optically stimulated and collected at a nearby p-n junction in the circuit. By monitoring the variation in the power supply current to the circuit, we can determine the logic state of a given circuit node. Unfortunately, this approach is invasive and can only observe well-defined logic states in the circuit.

Recently, a noninvasive back-side optical probing technique was demonstrated [14]. This system, referred to as the plasma-optical probing system, interferometrically detects the charge-induced index perturbation generated by electrical signals in the IC. Hence, it is capable of temporally and spatially resolving current and voltage waveforms at any internal node in an IC without any modification to the circuit or package. The high sensitivity of this approach has allowed previous researchers to detect both single-shot [14, 15] and picosecond stroboscopically sampled [16] signals. This concept has been shown to be useful for both bipolar [17] and MOS [18] ICs, and since the plasmaoptical effect is present in all semiconductor materials, this probing approach has found applicability in both silicon and GaAs ICs [19, 20].

This paper reviews the concept of plasma-optical probing of silicon ICs. The first section describes the physical basis for the plasma-optical effect from a classical viewpoint, and then discusses modifications to this analysis based on nonlinear material and quantummechanical considerations. The second and third sections describe the plasma-optical probing system, showing how it can be used to measure both internal current and voltage waveforms. The fourth section reviews the experimental results that have been demonstrated by various researchers with this system. Finally, the capabilities of the system are reviewed in Section 5. This last section demonstrates that the system has a high sensitivity and that it is noninvasive. With custom optics it should be possible to achieve submicron spatial resolution and thereby be able to probe future-generation high-performance ICs. In addition, the final section reviews the linearity of this approach and discusses the limitations to making calibrated measurements.

# 2. Plasma-optical effect

#### Classical analysis

The plasma-optical effect is based on the concept that electrons in the conduction band and holes in the valence band of a semiconductor behave very much as free carriers. From simple plasma physics, the local index of refraction is given [21] by

$$n = n_0 \sqrt{1 - \frac{q^2}{\epsilon \omega^2} \left[ \frac{N_c}{m_e^*} + \frac{N_h}{m_h^*} \right]}, \tag{1}$$

where  $N_{\rm e}$ ,  $m_{\rm e}$ ,  $N_{\rm h}$ , and  $m_{\rm h}$  are the electron and hole concentrations and effective masses, respectively. At optical frequencies, the index perturbation from the charge within a device is small. Therefore, by assuming that charge neutrality is maintained within the device being probed  $(\delta N_{\rm e} = \delta N_{\rm h})$ , and by defining a reduced mass given by  $m^* = m_{\rm e}^* m_{\rm h}^* / (m_{\rm e}^* + m_{\rm h}^*)$ , we can expand the index of refraction in a first-order Taylor series to obtain

$$n = n_0 \left( 1 - \frac{\omega_p^2}{2\omega^2} \right) = n_0 \left( 1 - \frac{q^2 N}{2\epsilon m^* \omega^2} \right), \tag{2}$$

where  $\omega_p^2 = q^2 N / \epsilon m^*$  is termed the plasma resonant frequency.

The plasma-optical probing system detects the index perturbation of Equation (2) by interferometrically sensing the differential phase shift between two optical beams—a probe beam, which passes through an active device, and a reference beam, which passes through a nearby region without a device. The differential phase shift experienced by the probe beam relative to the

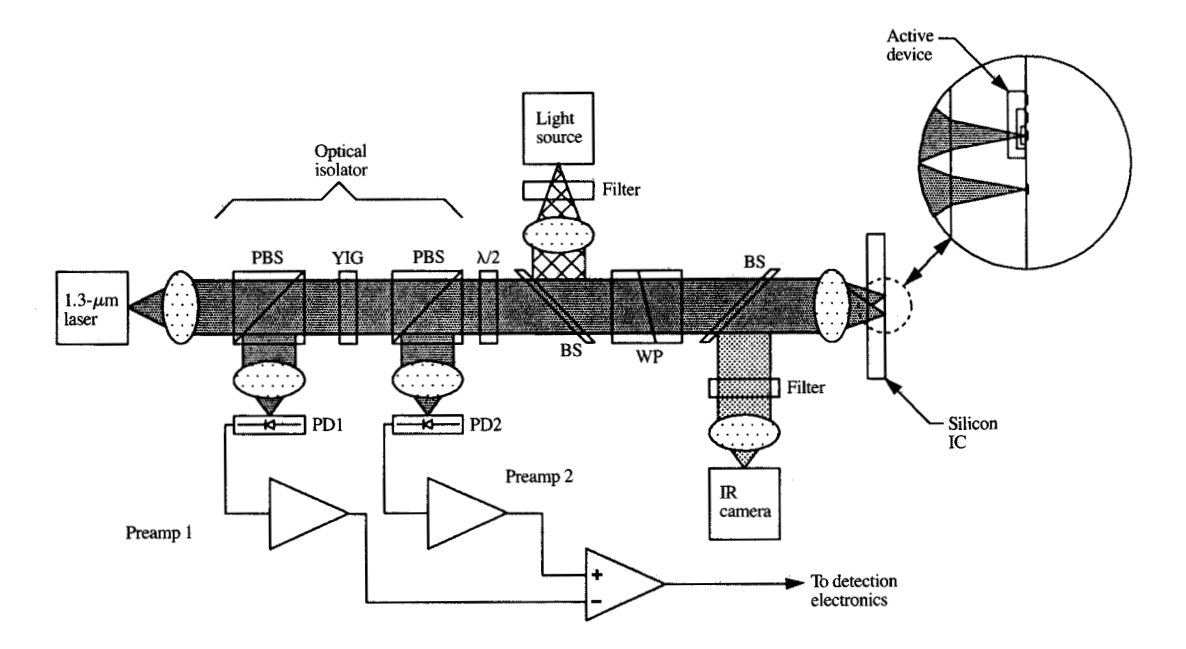


#### Figure 1

Optical schematic diagram of the charge-sensing probing system.

reference beam is given by

$$\delta\phi = \frac{2\pi\delta nL}{\lambda} = n_0 \frac{\omega_{\rm p}^2 \lambda L}{4\pi c^2}.$$
 (3)

Equation (3) shows that the differential phase shift measured with the plasma-optical probing system varies linearly with the charge-density modulation in the device and the wavelength of the probe beam. A more detailed analysis, which includes the effects of scattering and loss [21], shows that the absorption in this region varies as the square of the probe wavelength. Therefore, at optical frequencies that are far from the plasma resonant frequency and well below the bandgap of silicon, the optical loss can be very low; however, the charge-density modulation may still produce a significant phase shift.

#### Classical analysis modifications

In the above simple analysis, we assumed that the freecarrier effective mass was constant and independent of carrier concentration. However, Soref and Bennett [22] have applied the Kramers-Kronig relation between absorption and refractive index and have integrated available data for free-carrier absorption as a function of concentration. On the basis of their analysis, the freecarrier index perturbation was found to be slightly nonlinear with respect to the carrier concentration and given by

$$\delta n = \frac{n_0 q^2}{2\epsilon \omega^2} \left[ \frac{b_e N_e^{0.8}}{m_e^*} + \frac{b_h N_h^{1.05}}{m_h^*} \right]. \tag{4}$$

Koskowich et al. [23] have developed a detailed theoretical model for the interaction between free carriers and the optical probe beam that includes the various scattering and quantum-mechanical processes. Their theoretical analysis gave excellent agreement with experimental data for the absorption in silicon. However, this complex expression has yet to be integrated via the Kramers–Kronig relationship to obtain the refractive index perturbation [24]. Once this is done, this theoretical model should give an accurate expression for the refractive index perturbation.

## 3. Experimental system

Figure 1 shows a schematic diagram of the plasmaoptical probe. Light from a 1.3- $\mu$ m-wavelength laser diode is passed through an optical isolator, which prevents the optical beam from returning to the laser and generating excess noise. The light is then split into two beams by the Wollaston prism. The objective lens focuses the beams through the polished back side of the silicon IC into two spots on the front surface of the sample. One of the optical beams, the probe, is focused through an active device, a transistor or p-n junction, and reflects from the front-surface metallization. The other beam, the reference, passes through a region without an active device and is also reflected from the front-surface metallization. Both beams are recollimated by the objective lens and recombined by the Wollaston prism. Relative phase shifts between the probe and the reference change the polarization of the return optical beam. The polarizing beamsplitters in the optical isolator sense this polarization modulation and convert it to an amplitude modulation at the two photodiodes. A differential amplifier combines the out-of-phase signals from the two photodiodes and rejects any common-mode noise sources. We can observe the electrical signal from this system using either lock-in or wide-bandwidth single-shot detection techniques.

The relationship between the electrically induced refractive index perturbations in the IC and the signal observed at the photodetectors—i.e., the transfer function of the probe—can be analyzed by using optical ABCD or Jones matrices [25]. Using this approach, we can write the transfer function of the system as

$$\vec{E}_{o}^{+} = (J_{pv}R_{+}J_{W}[J_{r}J_{pv} + J_{po}J_{r}J_{po}J_{px}]J_{W}R_{+}J_{px})\vec{E}_{i}.$$
 (5)

The Jones matrices in the above expression are given by

$$J_{px} = \begin{bmatrix} 1 & 0 \\ 0 & 0 \end{bmatrix}, \qquad J_{py} = \begin{bmatrix} 0 & 0 \\ 0 & 1 \end{bmatrix},$$

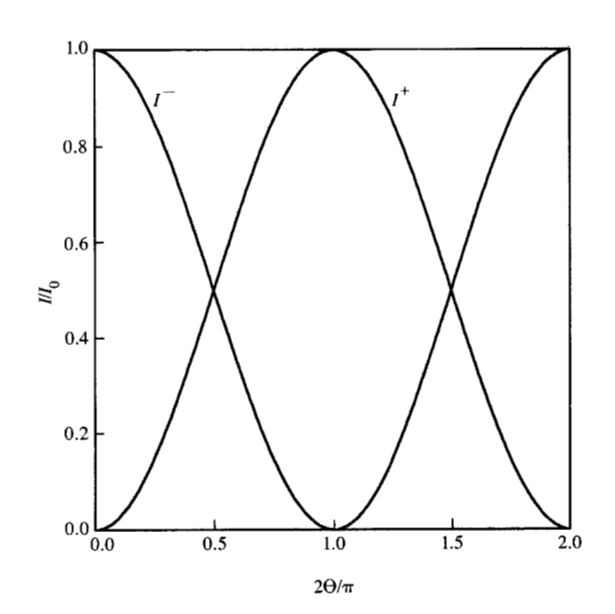
$$J_{w} = \begin{bmatrix} e^{j\Theta/2} & 0 \\ 0 & e^{-j\Theta/2} \end{bmatrix}, \qquad J_{po} = e^{j\phi} \begin{bmatrix} 1 & 0 \\ 0 & 1 \end{bmatrix}, \qquad (6)$$

$$R_{\pm} = \frac{1}{\sqrt{2}} \begin{bmatrix} 1 & \pm 1 \\ \mp 1 & 1 \end{bmatrix}, \qquad J_{r} = \begin{bmatrix} -1 & 0 \\ 0 & 1 \end{bmatrix};$$

where  $J_{\rm px}$  and  $J_{\rm py}$  are the Jones matrices of the x- and y-polarizing beam-splitters, respectively,  $J_{\rm w}$  is the Jones matrix of the Wollaston prism,  $J_{\rm po}$  is the Jones matrix of the plasma-optical effect,  $J_{\rm r}$  is the Jones matrix of the reflection from the metallization over the device in the IC, and  $R_{\pm}$  is the  $\pm 45^{\circ}$  rotation matrix to account for the physical orientation of the components in the system. Multiplying out the matrices in Equation (5), we can write the detected intensity at the first photodiode in terms of the round-trip static relative phase-shift (2 $\Theta$ ) between the probe and the reference beams and the plasma-optical phase shift ( $\phi$ ) as

$$I^{+} = I_0 \sin^2(\Theta + \phi). \tag{7}$$

The amplitude of the output from the second polarizer in the optical isolator is given by



#### Figure

Output of the two photodetectors of the charge-sensing optical probing system as a function of the relative phase shift between the probe and reference beams.

$$\vec{E}_{o}^{-} = (J_{px}R_{+}J_{w}[J_{r}J_{py} + J_{po}J_{r}J_{po}J_{px}]J_{w}R_{+}J_{px})\vec{E}_{i}.$$
 (8)

Again multiplying out these matrices, we can write the intensity at the second detector as

(6) 
$$I^{-} = I_{0} \cos^{2} (\Theta + \phi).$$
 (9)

Figure 2 shows a plot of the output at the two detectors as a function of the relative phase shift between the probe and the reference beams. From this figure, if the relative optical phase between the two beams is 0 or  $\pi$ , small-phase modulation from charge-induced index perturbations will generate very little intensity modulation at either detector. However, if the round-trip optical phase shift between the two beams is  $\pi/2$ , small-phase modulation from the charge-induced index perturbations will generate the maximum intensity modulation at both detectors. Under this condition, the small-signal intensity fluctuations at detector 1 are given by

$$\delta I^{+} = I_0 \phi, \tag{10}$$

and those at detector 2 are given by

$$\delta I^{-} = -I_0 \phi. \tag{11}$$

Since the outputs  $I^+$  and  $I^-$  are 180° out of phase, we can

165

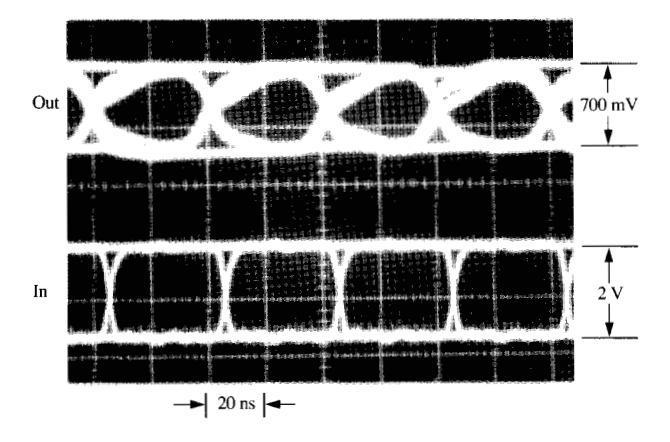


#### Figure 3

Optically detected 25-Mbit/s pseudorandom Manchester-coded bit stream applied to the base of a bipolar junction transistor. After B. R. Hemenway et al. [15], reproduced with permission. © 1988 IEEE.

difference these two signals to increase our signal strength and eliminate any common-mode noise signals present at both detectors, such as laser intensity fluctuations.

### 4. Experimental results

Charge-sensing optical probing systems have been used to detect single-shot [14, 15, 17] and repetitive signals [16] in high-speed silicon ICs. These systems have been used to detect electrical signals in both silicon and GaAs ICs [19, 20]. Measurements have been made in bipolar [14–16] ICs, and the prospect of measuring CMOS [18] ICs has been presented. This section reviews the key experimental results that have been achieved in this field.

# ◆ Single-shot signal detection

In a single-shot detection system, the plasma-optical probe can observe the signal in the integrated circuit without averaging. In this configuration, we effectively have an optical communication link between the device being probed in the IC and the photodiodes in the optical probing system; single transition events can thus be captured and observed with this type of system. With this capability, we can probe complex electrical waveforms in VLSI circuits, or catch random logic glitches. This type of signal cannot easily be recycled to accumulate an average, as is necessary in a stroboscopic signal detection system. However, since this approach uses widebandwidth photodiodes and amplifiers, the noise level in the measurement is much higher than for a stroboscopic system, and only very strong signals may be observed in this manner.

Despite these limitations, Hemenway et al. [15] have demonstrated an optical probing system with a 200-MHz

detection bandwidth, which exhibited a signal-to-noise ratio greater than 20 dB when probing the electrical signal in an 11  $\times$  11- $\mu$ m, 1-GHz  $F_{\tau}$  bipolar junction transistor. Figure 3 [15] shows an optically detected 25-Mbit/s pseudorandom Manchester-coded bit stream applied to the base of the transistor. In this particular configuration, modulation depths of 3-4% were achieved for 0.8-V ECL-level signals. Under higher drive conditions ( $I_c = 130 \text{ mA}$ ), modulation depths of nearly 10% could be achieved. These results show the highest modulation depth and widest bandwidth of any singleshot measurements made to date, and they were made with a low-power 1.3-μm semiconductor laser source. Since the signal-to-noise ratio is proportional to the square root of the optical probing power, we could potentially achieve a single-shot detection bandwidth of over 1 GHz with higher-power optical sources.

#### • Stroboscopic signal detection

When probing very-high-performance bipolar ICs or CMOS circuits with a low-power laser source, we observe a much smaller signal. In addition, the signal transition times in these circuits may occur in only a few picoseconds. Under these conditions, the stroboscopic signal-detection system provides a powerful means of measuring these signals. In this system, the measurement bandwidth is determined by the pulsewidth of the laser source; the detection bandwidth, which determines the noise in the measurement, can be independently set, and is only related to the offset frequency between the laser signal source and the electrical source to the IC [26]. Near-infrared lasers with very short optical pulsewidths have been demonstrated [27, 28] that would give this probing system the capability of detecting >100-GHzbandwidth electrical signals—i.e., virtually unlimited measurement bandwidth potential.

Using a 42-ps pulsed semiconductor laser source, Black et al. [16] have stroboscopically detected 1-GHz electrical signals in a 1.5- $\mu$ m × 5- $\mu$ m-emitter, 5-GHz  $F_{T}$  bipolar junction transistor. Figure 4 [16] shows the measurement made with this optical probing system. In this measurement, a 0.8-V electrical signal was applied to the base-emitter terminals of a device, which was biased to show clipping in the lower part of the waveform. Since this clipped signal has numerous harmonics, this measurement demonstrates the multigigahertz-bandwidth signal-detection capabilities of this system. Although the waveform shown in Figure 4 represents the accumulation of nearly a million signals, the display from this stroboscopic measurement system was refreshed at a rate of 33 Hz. This display rate was fast enough that the signals appeared in "real time"; when the optical beams were moved relative to the device, or the drive to the device was changed, these changes were immediately observed.

# 5. System capabilities

This section presents the capabilities of the chargesensing system and discusses the factors limiting its performance. The system's capabilities include its sensitivity, its noninvasiveness, spatial resolution limitations, linearity of the measurements, and signal calibration.

#### • Sensitivity

The sensitivity of the charge-sensing system depends upon two factors: the noise level in the detection system and the transfer function of the probing system. By carefully designing the system to minimize the various noise terms, researchers [15, 16] have demonstrated shotnoise-limited signal-detection capability. Under this condition, the rms noise-current signal at the photodiode is given by

$$\langle i \rangle = \sqrt{2qI_0B}, \tag{12}$$

where q is the charge on an electron,  $I_0$  is the static photocurrent, and B is the bandwidth of the detection system. To determine how much charge-density modulation is needed to achieve a signal-to-noise ratio of one, we can equate Equation (12) to the sum of Equations (10) and (11) in conjunction with Equation (3) to obtain

$$\delta N_{\rm s} = \delta N L = \frac{2\pi c^2 n_0 \epsilon_0 m^*}{q^2 \lambda} \sqrt{\frac{qB}{I_0}}, \qquad (13)$$

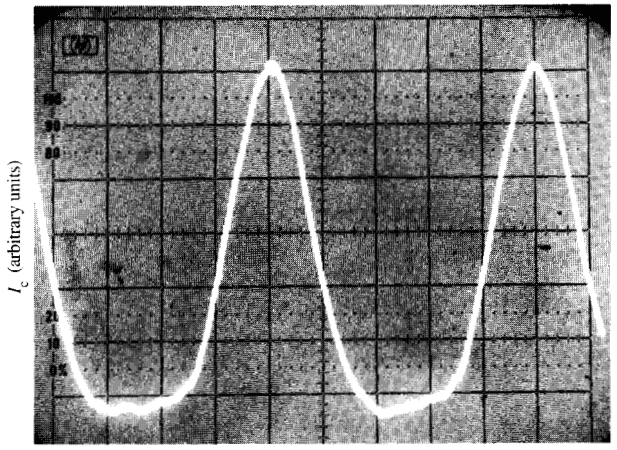
where  $I_0$  is the total photocurrent generated in both photodiodes. Equation (13) represents an effective sheet-charge density,  $\delta N_s$ , seen by the optical probing system as a result of integrating the volume-charge-density index perturbations along the path length L. This expression shows that as we use higher optical powers or a longer-wavelength probe beam, the system can detect smaller and smaller variations in internal charge density within devices in the circuit; i.e., the sensitivity of the system is improved. For a system photocurrent of  $I_0 = 1$  mA, the shot-noise-limited sheet-charge-density sensitivity of the system is given by

$$\frac{\delta N_{\rm s}}{\sqrt{\rm Hz}} = 1.3 \times 10^8 \, \frac{e}{\rm cm^2 \sqrt{\rm Hz}} \,. \tag{14}$$

Using Equation (4), Koskowich and Soma [18] have shown that the above expression should be modified by a value of

$$\gamma = \frac{1}{m^*} \left[ \frac{b_{\rm e} N_{\rm e}^{0.15}}{m_{\rm h}^*} + \frac{b_{\rm h} N_{\rm h}^{-0.20}}{m_{\rm h}^*} \right],\tag{15}$$

where  $\gamma$  varies from approximately 0.3 to 1.0 over an acceptor doping concentration range of  $N_{\rm A}=10^{15} \to 10^{18}$ 



200 ps/div

#### THIN SE

1-GHz stroboscopically detected electrical signal in a 5-GHz  $F_{\rm T}$  bipolar transistor. Transistor is biased to show waveform clipping. After A. Black et al. [16], reproduced with permission.

cm<sup>-3</sup>. Since this factor has not yet been experimentally verified, and since it would significantly improve the theoretical sensitivity of the measurement system, we use Equation (14) as a worst-case estimate of the sensitivity of the probe. Notice that even with this low optical power, the worst-case shot-noise-limited sensitivity represents the fluctuation of only a few electrons averaged over a second within a  $1-\mu m$  optical spot, and suggests that the interaction between free carriers and the optical probe is strong.

#### Probing current in a bipolar transistor

The relationship between the optical signal and the electrical signal in the IC depends upon where in the device the probe and reference beams are focused. Figure 5 shows a probing configuration for sensing the current through a bipolar junction transistor. In this configuration, the probe is focused on the emitter, and the reference is focused on the base of the device. Signals at the collector–substrate and collector–base junctions are common to both beams and are canceled. However, the base diffusion charge is sensed only by the probe. The relationship between this charge and the collector-current density is given by

$$q\delta N_{\rm s} = J_{\rm c} \tau_{\rm F} \,, \tag{16}$$

where  $\tau_{\rm F}$  is the base-emitter transit time. Transistor models [29] suggest that  $\tau_{\rm F}$  is constant over many decades of collector current. Therefore, in this configuration, the charge-sensing optical probe is a linear current probe. For an  $F_{\rm T}=5$  GHz,  $2\times5$ - $\mu$ m-emitter

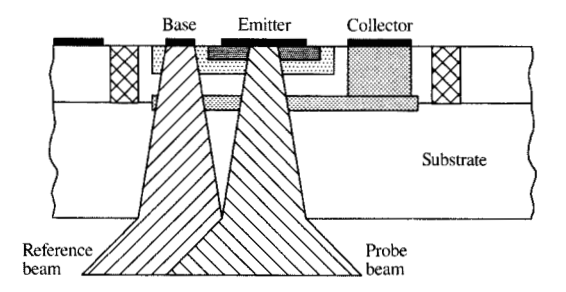


#### Figure 5

Position of the optical probe and reference beams for sensing the current through a bipolar junction transistor.

transistor and a system photodiode current of  $I_0 = 100$   $\mu$ A, the minimum detectable collector current is

$$\frac{I_{c_{\min}}}{\sqrt{Hz}} = \frac{145 \text{ nA}}{\sqrt{Hz}}.$$
 (17)

For a real-time display of this signal (30-Hz repetition rate), we typically need a detection bandwidth of  $\sim$ 1 kHz (to include all the signal harmonics); therefore, the sensitivity of this system (S/N = 1) for this device is

$$I_{c_{min}} = 4.6 \ \mu A.$$
 (18)

If this transistor were switching 1 mA of current, as in a typically ECL application, this signal would be observed with a S/N ratio of over 200. This example shows that using semiconductor lasers, this probing system can sense current signals in high-performance bipolar transistors and display them at conventional TV scan rates, with an excellent S/N ratio.

Probing voltage in a reverse-biased p-n junction Under reverse-biased conditions, a p-n junction stores varying amounts of charge in the depletion region of the device. The charge-density modulation in the junction is related to the small-signal voltage applied to the device by the capacitance per area, or

$$q\delta N_s = C'v_s \,. \tag{19}$$

For a one-sided step junction, the capacitance per area is given [30] by

$$C' = \sqrt{\frac{q\epsilon N_{\rm a}}{2(\phi_{\rm bi} - V_{\rm bias})}},\tag{20}$$

where  $N_a$  is the impurity concentration on the lightly doped side of the junction,  $\phi_{bi}$  is the junction built-in

potential ( $\sim$ 0.7 V), and  $V_{\rm bias}$  is the bias applied to the junction. Substituting Equation (19) in Equation (13), we can write the minimum detectable voltage in a reverse-biased p-n junction as

$$\frac{V_{\rm min}}{\sqrt{\rm Hz}} = \frac{2\pi c^2 n_0 \epsilon_0 m^*}{q \lambda} \sqrt{\frac{2(\phi_{\rm bi} - V_{\rm bias})}{\epsilon I_0 N_{\rm a}}}. \tag{21}$$

For a doping concentration of  $N_{\rm a}=10^6~{\rm cm}^{-3}$ , a reverse bias of  $V_{\rm bias}=0~{\rm V}$ , and a system photocurrent of  $I_0=100~\mu{\rm A}$ , the sensitivity of this probing system is

$$\frac{V_{\min}}{\sqrt{\text{Hz}}} = \frac{1.35 \text{ mV}}{\sqrt{\text{Hz}}}.$$
 (22)

This analysis suggests that 5-V signals in a CMOS IC could be displayed at a 30-Hz repetition rate with a S/N ratio of over 100. However, for typical 0.8-V signals in bipolar ECL circuits, the S/N ratio would only be between 10 and 20. Hence, a slower-rate display system (narrower detection bandwidth) and higher-power laser source would be necessary for making low-level voltage measurements.

# Noninvasiveness

Since the 1.3- $\mu$ m optical wavelength used for these measurements is well below the bandgap of silicon [31], the probe causes very little perturbation in the circuit. The effect of a high-powered solid-state laser source on a bipolar transistor has been experimentally measured [32]. The experiment showed that even for a 100-mW laser source, the collector current of the device was perturbed by less than 1  $\mu$ A. If we assume that the collector current was a result of optical absorption in the base region of the transistor, the base current perturbation ( $\beta = 150$ ) was less than 10 nA. Typical probing systems, using semiconductor lasers, operate with substantially less optical power ( $I_0 < 1$  mW) than the solid-state laser used in this experiment. Hence, the perturbation created by the optical probe within the integrated circuit is expected to be very small.

#### • Spatial resolution

The spatial resolution of the charge-sensing probe is limited by the achievable numerical aperture of the objective lens [33, 34], and is approximated by

$$w \approx \frac{\lambda}{NA},\tag{23}$$

where NA is the product of the index of refraction (the lowest between the objective lens and the sample) and the sine of the half-angle of the objective lens focus, and  $\lambda$  is the vacuum wavelength of the optical probe beam  $\lambda = 1.3 \ \mu m$ . Conventional immersion microscope lenses are available that have numerical apertures exceeding 1.0.

However, spherical aberration, generated by focusing through the substrate of the sample, limits the achievable spatial resolution of these lenses to  $1-2~\mu m$ . By thinning the substrate to minimize aberrations and by using custom optics, we should be able to achieve submicron spatial resolution.

#### • Linearity

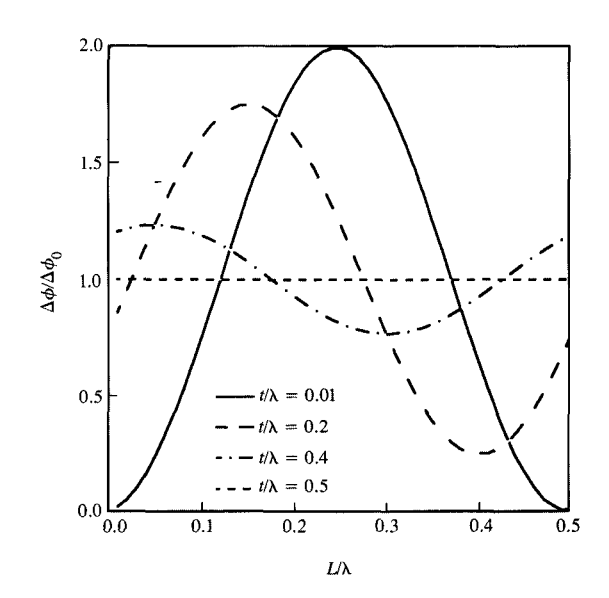
The nonlinearities in measuring charge with this optical probe arise from two sources: the nonlinear index-charge relationship, given classically by Equation (2), and the nonlinear intensity-phase relationship, given by Equation (7). Expanding these two expressions in a second-order Taylor series, we can write the small-signal intensity modulation at one of the photodetectors as

$$\frac{\delta I}{\delta I_1} = \left[ 1 + \frac{q^2 \delta N}{4\epsilon m^* \omega^2} + \frac{2}{3} \left( \frac{\lambda q^2 \delta N_s}{4\pi n_0 c^2 \epsilon_0 m^*} \right)^2 \right],\tag{24}$$

where  $\delta I_1$  is the linear theoretical small-intensity modulation from Equation (10). The second term in the bracket represents the nonlinearity introduced from high carrier concentrations, and the third term represents the nonlinearity introduced from high carrier-length products (sheet-charge densities). Assuming that the interaction length is  $L = \lambda/10$  and that the system photocurrent is  $I_0$ = 1 mA, we find that the linearity of the charge-sensing system is determined by the volume-charge density term. Under this condition,  $\delta I$  will be linear to within 1% with respect to the charge-density modulation over a 128-dB dynamic range relative to the shot-noise floor in a 1-Hz bandwidth. If the interaction length is increased, the nonlinearities introduced from the sheet-charge density will increase and eventually limit the dynamic range of the probe. This suggests that the charge-sensing probe is very linear with respect to the charge-density modulation in the IC over a very wide range of operation. However, a more exact analysis of the linearity of the charge-sensing system must contain the carrier-dependent effective mass from Equation (4), and would then be a function of the doping concentration. This analysis would cause a slight reduction in the linear dynamic range of this probing system. However, when measuring electrical signals, we encounter the greatest measurement nonlinearity from the charge-voltage or charge-current relationship of a particular device. A first-order correction of the charge and device nonlinearities could be made with appropriate hardware or software.

#### • Calibration

To calibrate the charge-sensing probe, we must ascertain the relationship between the electrical signals applied to the device in the circuit and the system photodetector. This transfer function depends upon the average



#### The state of the s

Normalized differential phase shift as a function of the location of the free-carrier region for various thicknesses of the charge region.

photocurrent in the system, the physical structure of the device, the optical interference effects in the probe and reference beams, and thermally generated index perturbations. By accounting for each of these effects, we should be able to develop a calibrated optical probe.

Interference effects between the forward- and backward-traveling optical beams in the device modify the magnitude of the plasma-optical effect. Since the amplitude of the optical electric field is zero at a null in the standing wave, we expect that the plasma-optical interaction will be zero for charge at a null. However, since the relative amplitude of the optical electric field is doubled at the peaks in the standing wave, we expect that the plasma-optical interaction will be twice as large for charge located there. For thick charge regions, the average plasma-optical interaction converges to the result presented in the classical analysis section. Between these two results, the phase shift accumulated by an optical beam traveling through a charge region of thickness t located a distance the form a perfect reflector is given by

$$\phi = 2 \tan^{-1} \left[ \frac{\tan(kl)\cos(n'kt) + \sin(n'kt)/n'}{\cos(n'kt) - n'\sin(n'kt)\tan(kl)} \right],$$
 (25)

where n' is the relative index of refraction of the region containing the free carriers. **Figure 6** shows a plot of the normalized differential phase shift through this region as a function of the longitudinal position for varying

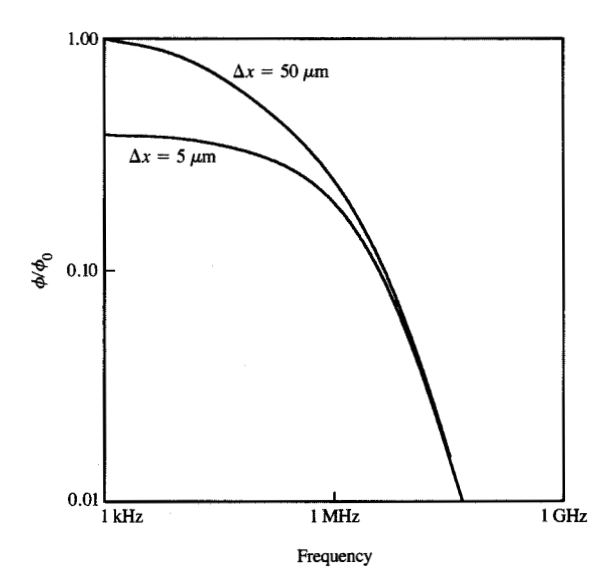


# Figure 7 Thermal signal frequency response.

thicknesses of the charge region. This figure shows that for very thin charge regions  $(t/\lambda \ll 1)$ , the sensitivity of the probe depends strongly upon the exact location of the free carriers, while for thick charge regions  $(t \gg 1000 \text{ Å})$ , the strength of this effect is diminished and eventually converges to the expected value. Since the thickness of the charge-density-modulation region near the edge of a p-n junction occurs over several Debye lengths [30], this effect is generally small for most devices. However, it becomes important in the probing of quantum-well structures.

The largest source of signal error in this measurement system is from the thermally generated index perturbations in the circuit. When an active device switches, it dissipates power and consequently heats up. In silicon, the index of refraction of the material is a function of temperature, and for small temperature fluctuations, the index perturbation is dn/dT = $1.5 \times 10^{-4}$  (SS). The optical probe integrates this temperature-induced index profile through the substrate thickness. Although this effect appears large in comparison to the plasma-optical effect, the IC takes a significant amount of time to heat up, and the close proximity of the probe and reference cancel most of the thermally generated signal. Therefore, the magnitude of the thermal effect depends upon the bandwidth of the electrical signal and the separation between the probe and reference spots.

By modeling the transistor in the circuit as a small hemisphere located a large distance from a hemispherical heat-sink, we can solve the spherical transient heat equation [32, 36]. The optical probe integrates the temperature-induced index profile along the two paths, separated by  $\Delta x$ , corresponding to the probe and reference beam positions. Figure 7 shows a normalized plot of the accumulated phase shift between the two beams as a function of the frequency of the applied thermal signal. For spot separations greater than 5  $\mu$ m, the frequency response of this signal is less than 1 MHz. Beyond this frequency, the strength of the thermal signal falls off as 1/f. In the time domain, the thermal signal causes the baseline of the signal from the plasma-optical probe to droop; the strength of the droop is related to the frequency of the electrical signal and the average power dissipation in the device. Since the stroboscopic optical probing system is limited to f > 100 MHz (for commercially available mode-locked lasers), this signal will not likely be a problem for these measurements. However, when probing low-frequency, high-power circuits, we must correct for this signal.

Several efforts have been made to demonstrate that this type of system can make calibrated measurements in either silicon [17] or GaAs [19] diodes. In these measurements, the optical transfer function of the probe was carefully measured and then compared with the expected signal based on measurements made with an electronic capacitance meter. In both cases the data showed excellent agreement with the expected results obtained from the capacitance meter. In addition, by applying a very small signal to the GaAs diode, Keller et al. [19] observed the sensitivity variations caused by the optical standing waves. However, even under very smallsignal modulation conditions, these variations were slight, probably since the Debye length in the material is a sizable fraction of the optical wavelength ( $\lambda = 1.3$  $\mu m/n_0$ ). By ignoring the optical standing-wave effects, Keller et al. [19] were able to demonstrate a measurement that had a mean value within 1% of the electrically measured signal and a standard deviation of 16%.

#### 6. Conclusions

This paper has presented a review of the charge-sensing optical probing system. Electrical signals in the IC were shown to modulate the carrier concentration in active devices such as transistors and diodes; the plasma-optical probing system uses probe and reference beams to interferometrically sense the carrier-concentration-induced index perturbation.

Researchers have experimentally used this optical probe for noninvasive detection of both wide-bandwidth, single-shot signals and picosecond stroboscopic signals. In the single-shot system, no averaging was used to recover

the optically detected signals, which were observed in a 200-MHz detection bandwidth. In the stroboscopic detection system, signals were displayed at a 30-Hz repetition rate with a measurement bandwidth of over 8 GHz. These measurements demonstrate that the chargesensing optical probing system is a sensitive measurement technique which can detect picosecond electrical signals in silicon circuits.

This paper has also reviewed the capabilities of this probing technique. The sensitivity analysis showed that it has a 145-nA/ $\sqrt{\text{Hz}}$  current sensitivity in typical bipolar junction transistors and 1.35-mV voltage sensitivity in typical CMOS circuits. For probing signals in typical ECL circuits, the charge-sensing probe has a sensitivity much higher than that of other noncontact probing approaches; for the CMOS circuits, the mV voltage sensitivity is similar to that of other noncontact probing systems. This section has also demonstrated that this technique is noninvasive and introduces only a few nA of current into a bipolar circuit, even with high probe power. The spatial resolution of this system is currently limited to approximately 1 µm by the capabilities of commercially available high-N.A. lenses. However, by using custom optics, we should be able to achieve submicron spatial resolution. The measurements made with this system are very linear with respect to chargedensity modulation within a device. In a bipolar transistor, the constant value of the base transit time over a wide range of operating conditions makes this probe linear with respect to current in the device. However, in a p-n junction, the nonlinear voltage-dependent capacitance must be accounted for. We should be able to do this with custom hardware or through software corrections. Finally, this paper has discussed the limitations to making calibrated measurements with this system. Both the thermally generated index perturbations and the optical standing waves in the probe and reference beams were found to create measurement errors. When probing typical devices, with charge regions larger than a few Debye lengths, the standing-wave effect was shown both theoretically and experimentally to cause only a minor perturbation. By using closely spaced probe and reference beams and limiting the system to detection of higher-frequency (f > 100 MHz) electrical signals, we can minimize the impact of the thermal effect, and should be able to make calibrated electrical measurements. Therefore, the charge-sensing optical probing system is a sensitive means of noninvasively detecting picosecond electrical signals in ICs, and it should prove to be a powerful tool for future circuit analysis.

#### References

 K.-Y. Toh, C.-T. Chuang, T.-C. Chen, J. D. Warnock, G.-P. Li, K. Chin, and T. H. Ning, "A 23ps/2.1mW ECL Gate,"

- presented at the IEEE International Solid State Circuits Conference, New York, February 15–17, 1989.
- V. A. Ranieri, A. Deutsch, G. V. Kopcsay, and G. Arjavalingam, "A Novel 24GHz Bandwidth Coaxial Probe," IEEE Trans. Instrum. & Measurement, to be published.
- G. Rabjohn, J.Wolczanski, and R. Surridge, "High-Frequency Wafer-Probing Techniques," Can. J. Phys. 65, 850 (1987).
- J. A. Valdmanis, G. A. Mourou, and C. W. Gabel, "Subpicosecond Electrical Sampling," *IEEE J. Quantum Electron.* OE-19, 664 (1983).
- H. Beha, H. Seitz, A. Blacha, and R. Clauberg, "Photoemission Sampling Technique for High-Speed Integrated-Circuit Testing," *Microelectron. Eng.* 7, 351 (1987).
- J. Bokor, A. M. Johnson, R. H. Storz, and W. M. Simpson, "High-Speed Circuit Measurements Using Photoemission Sampling," Appl. Phys. Lett. 49, 226 (1986).
- A. M. Weiner, P. S. D. Lin, and R. B. Marcus, "Picosecond Temporal Resolution Photoemissive Sampling," *Appl. Phys. Lett.* 51, 358 (1987).
- L. J. Fried, J. Havas, J. S. Lechaton, J. S. Logan, G. Paal, and P. A. Totta, "A VLSI Bipolar Metallization Design with Three-Level Wiring and Area Array Solder Connections," *IBM J. Res. Develop.* 26, 362 (1982).
- L. F. Miller, "Controlled Collapse Reflow Chip Joining," IBM J. Res. Develop. 13, 239 (1969).
- L. S. Goldman and P. A. Totta, "Area Array Solder Interconnections for VLSI," Solid State Tech. 26, 91 (1983).
- S. Sasaki, T. Kishimoto, and N. Matsui, "Connections of VLSI Chips to Printed Circuit Board Using Stacked Solder Bumps," Electron. Lett. 23, 1238 (1987).
- E. Ziegler and H. P. Feuerbaum, "IC Testing Using Optical Beam Induced Currents Generated by a Laser Scan Microscope," *Microelectron. Eng.* 7, 309 (1987).
- H. K. Heinrich, B. R. Hemenway, K. A. McGroddy, and D. M. Bloom, "Measurement of Real Time Digital Signals in a Silicon Bipolar Junction Transistor Using a Noninvasive Optical Probe," *Electron. Lett.* 22, 650 (1986).
- B. R. Hemenway, H. K. Heinrich, J. H. Goll, Z. Xu, and D. M. Bloom, "Optical Detection of Charge Modulation in Silicon Integrated Circuits Using a Multimode Laser-Diode Probe," Electron Device Lett. EDL-8, 344 (1987).
- A. Black, C. Courville, G. Schultheis, and H. K. Heinrich, "Optical Sampling of GHz Charge Density Modulation in Silicon Bipolar Junction Transistors," *Electron. Lett.* 23, 783 (1987).
- H. K. Heinrich, D. M. Bloom, and B. R. Hemenway, "Noninvasive Sheet Charge Density Probe for Integrated Silicon Devices," Appl. Phys. Lett. 48, 1066 (1986).
- G. N. Koskowich and M. Soma, "Optical Charge Modulation as an Internal Voltage Probe for CMOS IC's," *IEEE J. Quantum Electron*. OE-24, 1981 (1988).
- U. Keller, S. K. Diamond, B. A. Auld, and D. M. Bloom, "Noninvasive Optical Probe of Free Charge and Applied Voltage in GaAs Devices," Appl. Phys. Lett. 53, 388 (1987).
- G. N. Koskowich and M. Soma, "Voltage Measurement in GaAs Schottky Barriers Using Optical Phase Modulation," IEEE Electron Device Lett. EDL-9, 433 (1988).
- F. Wooten, Optical Properties of Solids, Academic Press, Inc., New York, 1972, pp. 52–55.
- R. A. Soref and B. R. Bennett, "Electrooptical Effects in Silicon," *IEEE J. Quantum Electron.* QE-23, 123 (1987).
- G. N. Koskowich, R. B. Darling, and M. Soma, "Effect of First-Order Phonon-Assisted Scattering on Near-Infrared Free-Carrier Optical Absorption in Silicon," *Phys. Rev. B* 38, 1281 (1988).
- 24. G. N. Koskowich, M. Soma, and R. B. Darling, "Near-Infrared

- Free-Carrier Optical Absorption in Silicon: Effect of First-Order Scattering in a Non-Parabolic Band," *Phys. Rev. B.*, to be published.
- E. Hecht and A. Zajac, Optics, Addison-Wesley Publishing Co., Reading, MA, 1976, pp. 268–271.
- B. K. Kolner and D. M. Bloom, "Electrooptic Sampling in GaAs Integrated Circuits," *IEEE J. Quantum Electron.* QE-22, 79 (1986)
- U. Keller, K. D. Li, M. Rodwell, and D. M. Bloom, "Noise Characterization of Femtosecond Fiber Raman Soliton Lasers," *IEEE J. Quantum Electron.* QE-25, 280 (1989).
- K. Tai and A. Tomita, "1100X Optical Fiber Pulse Compression Using Grating Pair and Soliton Effect at 1.319 μm," Appl. Phys. Lett. 48, 1033 (1986).
- I. Getreu, "Modeling the Bipolar Transistor," Tektronix Inc., Beaverton, OR, 1979, pp. 63-64.
- R. S. Muller and T. I. Kamins, Device Electronics for Integrated Circuits, John Wiley & Sons, Inc., New York, 1977, pp. 112– 128
- H. Y. Fan and M. Becker, "Infra-Red Absorption of Silicon," *Phys. Rev.* 78, 178 (1950).
- H. K. Heinrich, "A Noninvasive Optical Probe for Detecting Electrical Signals in Silicon Integrated Circuits," Ph.D. Thesis, Stanford University, Stanford, CA, 1987.
- J. W. Goodman, Introduction to Fourier Optics, McGraw-Hill Book Co., Inc., New York, 1968, pp. 101–140.
- G. S. Kino, "Fundamentals of Scanning Systems," Scanned Image Microscopy, E. A. Ash, Ed., Academic Press, Inc., New York, 1980, pp. 1–21.
- H. W. Icenogle, B. C. Platt, and W. L. Wolfe, "Refractive Indexes and Temperature Coefficients of Germanium and Silicon," Appl. Opt. 15, 2348 (1976).
- H. S. Carslaw and J. C. Jaeger, Conduction of Heat in Solids, 2nd Ed., Clarendon Press, Oxford, U.K., 1986, pp. 230–254.

Received May 26, 1989; accepted for publication August 17, 1989

Harley K. Heinrich IBM Research Division, Thomas J. Watson Research Center, P.O. Box 218, Yorktown Heights, New York 10598. Dr. Heinrich received his B.S.E. degree from Walla Walla College, College Place, Washington, in 1979, and the M.S.E.E. (1983) and Ph.D. (1987) in electrical engineering, both from Stanford University, Stanford, California. From 1979 to 1985 he was with Hewlett-Packard's optical communication division. In 1985, he received a Hewlett-Packard Fellowship and began his Ph.D. research on optical testing of high-speed silicon ICs. In 1987, Dr. Heinrich joined the IBM Thomas J. Watson Research Center as a Research Staff Member. His research interests include the application of high-speed electro-optics to the measurement of signals in integrated devices, circuits, and package structures. Dr. Heinrich is a member of the American Physical Society, the IEEE Lasers and Electro-Optics Society, and the Optical Society of America.